An Improved Fault Detection Method based on HSMM: Application to a Chemical Process

Lestari Handayani[1,3], Pascal Vrignat[2*], and Frédéric Kratz[3]

[1]*Universitas Islam Negeri Sultan Syarif Kasim Riau, Informatics Engineering, 28293, Pekanbaru, Indonesia*
lestari.handayani@uin-suska.ac.id

[2*]*Univ. Orléans, PRISME, EA 4229, F45072, Orléans, France*
pascal.vrignat@univ-orleans.fr

[3]*INSA-CVL, PRISME, EA 4229, F18020, Bourges, France*
frederic.kratz@insa-cvl.fr

ABSTRACT

This paper proposes a fault detection method for multivariate statistical process control. The proposed method combines the Forward-Backward Hidden Semi-Markov Model (HSMM) and Principal Component Analysis (PCA). A stochastic automaton was used for multi-mode detection with many observation sequences. We used agglomerative clusters to find the initial parameters of HSMM. We allocated an adaptive threshold and a fixed threshold in each mode for fault detection with PCA, including Hotelling T^2 statistic and squared predictive error (Q statistic). We simulated this method on the Tennessee Eastman Process (TEP). Some faults were designed with various runs and times of occurrence. The experimental results were compared with the Mixture Bayesian PCA, Hidden Markov Model (HMM), and HSMM methods. The results are robust with an efficient detection rate. This activity recommends ways to find action plans for multi-mode process monitoring in chemical plants.

1. INTRODUCTION

Radical advances in manufacturing technology have led to Industry 4.0 transformation, resulting in the emergence of complex industrial plants. Abnormal events in factories should be detectable with reference to process behavior measurements. Fault detection and process monitoring are necessary to estimate malfunctioning operations. The goal is to ensure that the system operates reliably and produces high-quality products with complete safety. Therefore, industrial processes need to be monitored in order to be modeled. However, as industrial plant processes become increasingly complex, developing accurate models becomes difficult and time-consuming.

Several approaches have been developed to detect abnormal process events, such as Multivariate Statistical Process Control (MSPC). The MSPC approach is a data-driven technique (Nawaz *et al.*, 2021). It has the advantage of not requiring a system model, only the availability of large amounts of historical process data. It is appropriate for systems that are complex, never modelled, or whose models are hybrid, nonlinear or unstructured. This approach can detect additive faults and multiplicative faults (Alkaya & Eker, 2011).

MSPC methods are algorithms that can extract essential information from large multivariable data sets (Jiang *et al.*, 2019). MSPC has been intensively studied as a technique for fault detection and recognition. Principal Component Analysis (PCA), (Xia *et al.*, 2021), Partial Least Squares (PLS), (Pratley *et al.*, 2015), and Canonical Correlation Analysis (CCA), (Wu *et al.*, 2020) methods have played a significant role in multivariate process monitoring using MSPC (Odiowei & Cao, 2009). Many industrial processes use multiple operational settings and transitions due to the variety and non-linearity of the variables. As a result, error detection in this process will lead to unreliable results and many missed diagnoses. Therefore, to address these limitations, the conventional MSPC approaches need to be improved. In this research, we merge the PCA and Markov model to improve the multi-mode process's fault detection capability. Numerous sophisticated PCA methods have been proposed in the literature and PCA has been successfully implemented in online continuous process monitoring (Nawaz *et al.*, 2021),

(Bakdi & Kouadri, 2018). Fault detection using PCA is usually performed by monitoring the Squared Prediction Error (SPE) (Q statistic) and/or Hotelling's T^2 statistic because they are able to detect irregularities that occur in process data (Nawaz *et al.*, 2021).

Mode identification in multi-mode processes (Lou & Wang, 2017), (Wang *et al.*, 2016), data-driven models (Peng *et al.*, 2017) such as the Markov model (Liu & Zhu, 2020) can be used to plan the maintenance policies (Vrignat *et al.*, 2022). HMMs have been successfully implemented in Prognostics and Health Management (PHM) systems (Atamuradov *et al.*, 2017), especially for improving the failure detection accuracy of machines operating under various operating conditions (Quatrini *et al.*, 2020). In general, HSMM is preferred because it guarantees a more realistic implementation when compared to Markov chains.

We will study the Tennessee Eastman Process (Md Nor *et al.*, 2020), a benchmark in chemical engineering research for failure detection, fault diagnosis and decision support systems (Reinartz *et al.*, 2021). It is very useful for device safety purposes in large-scale chemical plants. Several methods have been used to assess the data, such as Support Vector Machine (SVM) (Kulkarni *et al.*, 2005), deep learning (Kong & Ge, 2021), HMM (Wang *et al.*, 2016), and an HMM-Bayesian network hybrid model (Galagedarage Don & Khan, 2019). In the mode detection stage, we propose to use HSMM. The initial values of the HSMM parameters are obtained from the clustering results using agglomerative clustering. Movement between clusters can be considered as mode transitions. In each mode, we monitor the data using PCA and try to find the normal threshold for fault detection. Several statistical calculations are performed such as T^2 and Q using adaptive and fixed thresholds. The experimental results on TEP data will be compared with Mixture Bayesian PCA (MBPCA) (Ge & Song, 2010), HMM (Wang *et al.*, 2016) methods, and HSMM (Lou & Wang, 2017).

We contribute to the improvement of fault detection rate results using the TEP case study with fault scenarios from Lou and Wang (Lou & Wang, 2017). The main contributions of this paper are as follows. We:

1. Developed a Markov model approach by combining HSMM and PCA to optimize fault detection in a multi-mode process. The HSMM method used is Forward-Backward HSMM. In the initial stage of HSMM, Agglomerative Clustering is performed to initialize the HSMM parameters.

2. Propose several indices for fault monitoring by combining fixed and adaptive thresholds of PCA statistics.

3. Improved the Fault Detection Rate (FDR) for monitoring compared to previously published results.

The remaining sections are organized as follows. The second section describes HSMM theory. The third section presents PCA, T^2, and Q statistics and adaptive parameters. The following section describes the proposed approach. Section 5 describes the TEP process, multi-operational conditions, and failure detection examples. The results are discussed in Section 6, while the conclusions are presented in Section 7.

2. HIDDEN SEMI-MARKOV MODEL

Assume a semi-Markov process in discrete time with a set of hidden states (S). The state sequence $Q = \{s_1,...,s_T\}$ at time T. The observation sequence $O = \{o_1,...,o_T\}$ is denoted by o_1^T where $o_t \in V$. V is a set of observations $V = \{v_1,...,v_k\}$, with k is number of observations. The following parameters characterize this semi-Markov chain:

- Initial probabilities $\pi = \{\pi_m\}$ where $\pi_m = P(s_1 = m)$ with $\sum_m \pi_m = 1$;

- Transition probabilities $A = \{a_{mn}\}$ where $a_{mn} = P(s_{t+1} = n \mid s_t = m)$ with $\sum_{m \neq n} a_{mn} = 1$ and $a_{mm} = 0$;

- Observation or emission probabilities $B = \{b_m(v_k)\}$ where $b_m(v_k) = P(o_t = v_k \mid q_t = s_m)$;

- Duration probabilities $p = \{p_{md}\}$ where $p_{md} = P(s_{t+1:t+d} = m \mid s_{t+1} = m)$.

The model HSMM is defined as $\lambda_{HSMM} = (A, B, p, \pi)$.

Yu and Kobayashi (Yu & Kobayashi, 2003) proposed a Forward-Backward (FB) algorithm for the practical implementation of explicit-duration HMMs. First, it is necessary to define various probability conditions for the smoothed, filtered, and predicted estimates of the state. The Forward and Backward variables are then calculated with the modified FB algorithm. In addition, the HSMM parameter re-estimation method was refined through model training.

3. PRINCIPAL COMPONENT ANALYSIS

PCA transforms a set of interrelated variables into a set of uncorrelated variables called principal components, while retaining as much of the information in the original data as possible (Jolliffe & Cadima, 2016). This method is often used to explore relationships between variables, to simplify the analysis of complex data, and to visualize the data in a reduced dimensional space. Before applying PCA, data must be normalized. Consequently, the normalized process data matrix X can be decomposed as follows:

$$X = TP^T + E \in \square^{n \times s} \qquad (1)$$

$T \in R^{n \times \rho}$ is the score matrix, $P \in R^{s \times \rho}$ refers to the loading matrix, and $E \in R^{n \times s}$ is the residuals matrix. Where: n

symbolizes the number of samples, s symbolizes the number of variables, ρ is the principal components (PCs) number of the model.

When PCA is used, the PCs retained are frequently synthesized using the Hotelling T^2 statistic and the residuals are condensed using the Q statistic or Squared Predictive Error (SPE). The detection is performed by comparing the expected behavior to the output of the PCA model. The T^2 and Q statistics can be calculated using equations (3) and (4). However, previously the initial data X must be normalized to y using formula (2). Each data value x_{is} minus the mean x_s and divided by the standard deviation σ_s of n observations of variable s.

$$y_{i,s} = \frac{x_{is} - \overline{x_s}}{\sigma_s} \tag{2}$$

$$T^2 = yP(\Lambda)^{-1}P^T y^T \tag{3}$$

$$Q = y(I - PP^T)(I - PP^T)y^T \tag{4}$$

where y is a normalized monitoring vector; I is the identity matrix; $\Lambda = diag(\lambda_1, \lambda_2, ..., \lambda_\rho)$ is the estimated covariance matrix of principal component scores that contains the eigenvalues (λ).

PCA statistics that use a fixed threshold of a certain significance level will control the rate of exchange between false alarms and missed detection rates. The process is considered faulty if the Q and T^2 statistics exceed the fixed control limits of Q_α and T_α^2, respectively (Bakdi & Kouadri, 2018). These thresholds are captured by applying the appropriate distribution law at an adapted confidence level (1- α) (Zhang *et al.*, 2019).

$$Q_\alpha = \theta_1 \left(1 + \frac{c_\alpha h_0 \sqrt{2\theta_2}}{\theta_1} + \frac{h_0 \theta_2 (h_0 - 1)}{\theta_1^2} \right)^{\frac{1}{h_0}} \tag{5}$$

with $h_0 = 1 - \dfrac{2\theta_1 \theta_3}{3\theta_2^2}$ and $\theta_i = \sum_{j=r+1}^{\rho} \Lambda_j^i$, $i = 1, 2, 3,$ (6)

where c_α is the critical value of the normal distribution for a level of confidence of (1- α), α is the level of significance, and r is the number of PCs selected. h_0 and θ are related to approximation of a sum of chi-square variates.

The fixed threshold T_α^2 is given in formula (7).

$$T_\alpha^2 = \frac{(g^2 - 1)l}{g(g - l)} F_\alpha(l, g - l) \tag{7}$$

where $F_\alpha(l, g - l)$ is the critical value at a relevance level α with l and g-l degrees of freedom of the Fisher-Snedecor distribution. The variables l, g and α are the number of PC, the number of samples and the acceptable false alarm rate, distinctly. The threshold still has drawbacks if it is set too high or too low. This will increase false detection and/or missed error detection.

Another method is the adaptive threshold scheme. This method is based on a modified Exponentially Weighted Moving Average (EWMA) control chart with a limited window length applied for the Q and T^2 error detection indices (Nawaz *et al.*, 2021). This threshold scheme uses historical statistics and generates a range of dynamic values above and below the fixed control limits to properly measure deviations in process operation. We will examine the use of fixed and adaptive thresholds on TEP.

Q_j^{ad} and $T_j^{2,ad}$ are the adaptive thresholds for the Q and T^2 statistic at the jth sample (Bakdi & Kouadri, 2018).

$$Q_j^{ad} = \max \left\{ \frac{1}{c_q^{w_q}} \left(Q_\alpha \sum_{i=1}^{w_q} c_q^i - \sum_{i=1}^{w_q - 1} c_q^i q_{j - w_q + i} \right), 0.2 Q_\alpha \right\} \tag{8}$$

$$T_j^{2,ad} = \max \left\{ \frac{1}{c_t^{w_t}} \left(T_\alpha^2 \sum_{i=1}^{w_t} c_t^i - \sum_{i=1}^{w_t - 1} c_t^i t_{j - w_t + i} \right), 0.2 T_\alpha^2 \right\} \tag{9}$$

where w_t and c_t are window adjustment period and weight factor for the T^2 statistic, distinctly. The filtered j^{th} sample is given by:

$$q_j' = \frac{\sum_{i=1}^{w_q} c_q^i q_{j - w_q + i}}{\sum_{i=1}^{w_q} c_q^i} \tag{10}$$

The parameter c_q is a weighting item greater than 1, and it determines the rate at which older samples enter into the calculation of q_j'. The filter window length is represented by w_q for the Q fault detection index; i.e., it is the number of samples used by the filter. With this approach, the jth sample is considered faulty if $q_j' > Q_\alpha$.

4. PROPOSED METHODOLOGY

The flowchart of proposed method is illustrated in Figure 1. The anomaly detection process begins with offline learning of data considered normal or healthy. Subsequently, the process can be applied to test data that may contain anomalies to be detected. These are the offline model training steps:

1) Agglomerative clusters are constructed from linkages (Nielsen, 2016). A *linkage* is the distance between two clusters. Ward's linkage is used to create a hierarchical cluster tree. Ward's linkage is based on the incremental sum of squares, which is the increase in the total within-cluster sum of squares caused by joining two clusters. The sum of squares metric is equivalent to the distance metric $d(r,s)$, which is defined by the formula:
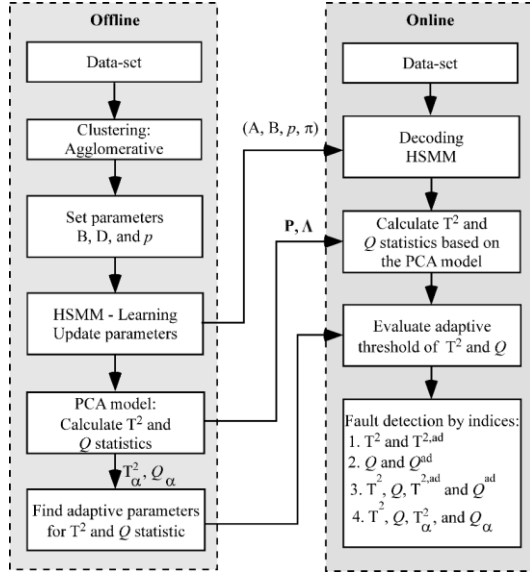
Figure 1. Flowchart of proposed method

$$d(r,s) = \sqrt{\frac{2n_r n_s}{(n_r + n_s)}} \left\| \overline{x}_r - \overline{x}_s \right\|_2 \qquad (11)$$

where:

$\| \ \|_2$ is the Euclidean distance.

$\overline{x}_r$ and $\overline{x}_s$ are the centroids of clusters r and s.

n_r and n_s are the number of elements in clusters r and s.

2) Initialization of HSMM parameter values. We give initial values for A, B, p, and π. A vector of π and matrix of A can be set randomly to satisfy $\sum_m \pi_m = 1$, $\sum_{m \neq n} a_{mn} = 1$, and $a_{mm} = 0$. It is possible to use the results of the clustering technique to assign initial values to the B matrix. We assume that the data in each operation mode obey a unimodal Gaussian distribution, $x_i \ N (\mu_i, \Sigma_i), \quad i = 1, 2, ..., M$. The maximum duration in each state (D_i) and D_{max} is the longest sojourn time of all states. So, the p vector can be set as a random vector compliant with the condition $\sum_{t=1}^{D_{max}} p_i(t) = 1$. After finding the right cluster result, the initial value of HSMM can be calculated. Where cluster displacement can be considered as state transition (A), and we can calculate the emission probability (B), maximum duration of each state (D_i) and duration probability (p).

3) Forward-Backward HSMM (FB HSMM) training the healthy data to obtain updated parameter values. The FB HSMM algorithm is as follows:

Algorithm: FB HSMM

Input: model $\lambda_{\text{HSMM}}(A, B, p, \pi)$

  for t=1 **to** T **do**   % Forward recursion:

    Forward variable calculation $\alpha_{t|t-1}(m,d)$:

    if t=1 **then** $\alpha_{1|0}(m,d) = \pi_m p_m(d)$

    else $\alpha_{t|t-1}(m,d) = \vartheta_{t-1}(m) p_m(d) + b_m^*(o_{t-1}) \alpha_{t-1|t-2}(m, d+1)$

    Calculation of filtered probability ratio $b_m^*(o_t)$:

$$b_m^*(o_t) \overset{def}{=} \frac{\alpha_{t|t}(m,d)}{\alpha_{t|t-1}(m,d)} = \frac{b_m(o_t)}{P(o_t \mid o_1^{t-1})}$$

    Probability function of the observation sequences:

$$P(o_1^T) = \left(\prod_{t=1}^{T} r_t\right)^{-1}, \text{ where } \quad r_t^{-1} \overset{def}{=} P(o_t \mid o_1^{t-1}) = \sum_{m,d} \alpha_{t|t-1}(m,d) b_m(o_t) = \sum_m \gamma_{t|t-1}(m) b_m(o_t)$$

    Calculation of the conditional probabilities of a state starting at $t+1$ given o_1^t:

$$\varepsilon_t(m) \overset{def}{=} P(q_t = s_m, \tau_t = 1 \mid o_1^t) = \alpha_{t|t-1}(m,1) b_m^*(o_t)$$

    Calculation of the conditional probabilities of a state ending at t given o_t:

$$\vartheta_t(m) \overset{def}{=} P(\tau_t = 1,) q_{t+1} = s_m \mid o_1^t) = \sum_n \varepsilon_t(n) a_{nm}$$

    end if

  end for

  for t=T **down to** 1 **do**   % Backward recursion

    Calculation of filtered probability ratio $b_m^*(o_t)$:

$$b_m^*(o_t) \overset{def}{=} \frac{\alpha_{t|t}(m,d)}{\alpha_{t|t-1}(m,d)} = \frac{b_m(o_t)}{P(o_t \mid o_1^{t-1})}$$

Backward variable calculation $\beta_t(m,d)$:

if t=T **then** $\beta_T(m,d) = b_m^*(o_T)$

else $\beta_t(m,d) = \begin{cases} \vartheta_{t+1}^*(m)b_m^*(o_t), & d=1 \\ \beta_{t+1}(m,d-1)b_m^*(o_t), & d>1 \end{cases}$

$$\varepsilon_t^*(m) \overset{def}{=} \frac{P(o_t^T \mid q_t = s_m, \tau_{t-1} = 1)}{P(o_t^T \mid o_1^{t-1})}$$

$$= \sum_d p_m(d)\beta_t(m,d)$$

$$\vartheta_t^*(m) \overset{def}{=} \frac{P(o_t^T \mid q_{t-1} = s_m, \tau_{t-1} = 1)}{P(o_t^T \mid o_1^{t-1})}$$

$$= \sum_n a_{mn}\varepsilon_t^*(n)$$

end if
end for
return $\alpha_{t|t-1}(m,d), \beta_t(m,d), b_m^*(o_t), \varepsilon_t(m), \vartheta_t(m), \varepsilon_t^*(m), \vartheta_t^*(m)$

The marginal probability distribution of $q_t = s_m$, which is denoted by the variable γ.

$$\gamma_{t|x}(m) \overset{def}{=} \sum_d \alpha_{t|x}(m,d) \tag{12}$$

The smoothed probability of state s_m to state s_n at t is denoted by:

$$\theta_{t|T}(m,n) = \varepsilon_{t-1}(m)a_{mn}\varepsilon_t^*(n) \tag{13}$$

And the probability that state m is included at t and lasts for d time units is:

$$\phi_{t|T}(m,d) = \vartheta_{t-1}(m)p_m(d)\beta_t(m,d) \tag{14}$$

Hidden states that start at time t can be considered with the maximum posterior (MAP) using equation (15).

$$(q_t, \theta_t) \overset{def}{=} \arg\max_{(m,d)} P(s_m \; start \; at \; t, \tau_t = d \mid o_1^T) \\ = \arg\max_{(m,d)} \vartheta_{t|T}(m,d) \tag{15}$$

The re-estimated model parameters are:

$$\hat{a}_{mn} = \frac{\sum_t \theta_{t|T}(m,n)}{\sum_n \sum_t \theta_{t|T}(m,n)} \tag{16}$$

$$\hat{b}_m(v_k) = \frac{\sum_t \gamma_{t|T}(m)I(o_t = v_k)}{\sum_t \gamma_{t|T}(m)} \tag{17}$$

$$\hat{p}_m(d) = \frac{\sum_t \phi_{t|T}(m,d)}{\sum_d \sum_t \phi_{t|T}(m,d)} \tag{18}$$

$$\hat{\pi}_m = \frac{\gamma_{1|T}(m)}{\sum_m \gamma_{1|T}(n)} \tag{19}$$

4) Calculation of T^2, Q, Q_α, and T_α^2 statistics of the training data using the formulas (3), (4), (5), (7), respectively. We calculate it for each state. The eigenvectors and eigenvalues from this step will be operated for the calculation of T^2 and Q in the online step with the new test data.

5) Identifying adaptive parameters for T^2 and Q, i.e., an adaptation window length that ensures adequate sample averaging and an adaptation weighting factor that results in a false alarm rate of 0% in the training set. In the online step, these parameters will be adopted to evaluate the test data threshold.

The steps for the online monitoring of test data are as follows:

1) Input test data: real-time test data that may contain healthy and failed data.

2) Decoding HSMM: given the observation o_1^T, we can estimate the hidden states that start at time t by equation (14).

3) Calculation of T^2 and Q statistics. This calculation uses the eigenvalues and eigenvectors derived from the training process. This applies to the estimate for each state.

4) Evaluate the adaptive threshold of T^2 and Q: it evaluates the T^2 and Q of the test data using T_α^2, Q_α, $T^{2,ad}$, and

Q^{ad} from the training data. This method is carried out in each estimation state.

5) Fault detection by some indices:

    a. Fault detection based on T^2 and $T^{2,ad}$. Using the T^2 adaptive threshold, a fault is detected when one of the samples T^2 statistics exceeds the corresponding adaptive threshold set.

    b. Fault detection using Q and Q^{ad}. A fault is identified when one of the sample Q statistics exceeds the respective adaptive threshold.

    c. T^2, Q, $T^{2,ad}$, and Q^{ad} indices are used for fault detection. We combine the two statistics, thus simplifying the fault detection process:

$$CI_{ad} = z*\left(\frac{T^2}{T^{2,ad}}\right) + (1-z)*\left(\frac{Q}{Q^{ad}}\right) \qquad (20)$$

where z is 0.5 to balance SPE (Q) and T^2. The process is diagnosed as faulty if $CI_{ad} > 1$.

    d. *The indices* T^2, Q, T_α^2, *and* Q_α.

It combines the indices of T^2, Q, T_α^2, and Q_α for fault detection:

$$CI_\alpha = z*\left(\frac{T^2}{T_\alpha^2}\right) + (1-z)*\left(\frac{Q}{Q_\alpha}\right) \qquad (21)$$

where z is 0.5 to balance Q and T^2. The process is considered faulty if $CI_\alpha > threshold$. The *threshold* value is obtained from the experimental data.

5. TENNESSEE EASTMAN PROCESS

This section applies the suggested methodology to the Tennessee Eastman Process (TEP). This system offers a realistic industrial process for evaluating process control and monitoring techniques (Downs & Vogel, 1993; Tamssaouet *et al.*, 2019). This system incorporates five major functions: a reactor, condenser, compressor, separator, and stripper, as well as eight components: A, B, C, D, E, F, G, and H. The gaseous reactants A, C, D, and E, along with the inert B, are incorporated into the reactor, where the liquid products G and H are manufactured (Reinartz *et al.*, 2021). F is elaborated as a by-product of the reactions.

Scheme 1. The reactions in the reactor are:

$$
\begin{aligned}
A(g) + C(g) + D(g) &\rightarrow G(liq), &&\text{Product 1,} \\
A(g) + C(g) + E(g) &\rightarrow H(liq), &&\text{Product 2,} \\
A(g) + E(g) &\rightarrow F(liq), &&\text{Byproduct,} \\
3D(g) &\rightarrow 2F(liq), &&\text{Byproduct,}
\end{aligned}
$$

The reactions involved in this process are exothermic, irreversible, and approximately first order with respect to the concentrations of the reactants. The reaction rates are temperature dependent and follow Arrhenius functions. The G reaction requires a higher activation energy than the H reaction, making it more temperature sensitive. In sum, the product stream is cooled before being directed to a vapor-liquid separator. The steam produced is then recycled through a compressor to maximize the use of raw materials. However, a portion of this stream is purged regularly to avoid the accumulation of inert gases and by-products in the reactor. The condensed components (Stream 10) from the separator are pumped to a stripper. Stream 4 is employed to strip Stream 10 of any remaining reactants, which are then combined with the recycled stream via Stream 5. The stripper's base-exiting G and H products are routed to a process not depicted in the diagram (Figure 2). A revision of TEP was detailed in (Bathelt *et al.*, 2015). Figure 2 shows the piping and instrumentation diagram (P&ID) of the system with expanded measurements.

Figure 2. A process flowsheet for the TEP

Data generated by simulation of updated TE code (https://depts.washington.edu/control/LARRY/TE/download.html, January 23, 2015). The Simulink models can be used for the multi-loop strategies. We used MultiLoop_mode3 Simulink which is a closed-loop with control set points. This procedure introduces the three modes (Mode-1, Mode-2 and Mode-3) shown in Table 1 in order to test multi-mode approaches. The other parameter values for the three modes are identical.

Setpoint Label	Mode-1	Mode-2	Mode-3
Production	22.89	22.89	18,40
Mol % G	50	60	50
Separator level	40	50	50

Table 1. Three process operation modes in the TEP

There are 12 manipulated input variables (XMV1 to XMV12) and 73 measured output variables (XMEAS1 to XMEAS73) in the simulated model. The data under consideration include 31 variables listed in (Table 2).

No	Variable	Description
1.	XMV1	D feed flow valve at stream 2
2.	XMV2	E feed flow valve at stream 3
3.	XMV3	A feed flow valve at stream 1
4.	XMV4	Total feed flow valve at stream 4
5.	XMV6	Purge valve at stream 9
6.	XMV7	Separator pot liquid flow valve at stream 10
7.	XMV8	Stripper liquid product flow valve at stream 11
8.	XMV10	Reactor cooling water flow
9.	XMV11	Condenser cooling water flow
10.	XMEAS1	A feed at stream 1
11.	XMEAS2	D feed at stream 2
12.	XMEAS3	E feed at stream 3
13.	XMEAS4	Total feed at stream 4
14.	XMEAS5	Recycle flow at stream 8
15.	XMEAS6	Reactor feed rate at stream 6
16.	XMEAS7	Reactor pressure
17.	XMEAS8	Reactor level
18.	XMEAS9	Reactor temperature
19.	XMEAS10	Purge rate at stream 9
20.	XMEAS11	Product separator temperature
21.	XMEAS12	Product separator level
22.	XMEAS13	Product separator pressure
23.	XMEAS14	Product separator under flow at stream 10
24.	XMEAS15	Stripper level
25.	XMEAS16	Stripper pressure
26.	XMEAS17	Stripper underflow at stream 11
27.	XMEAS18	Stripper temperature
28.	XMEAS19	Stripper steam flow
29.	XMEAS20	Compressor work

No	Variable	Description
30.	XMEAS21	Reactor cooling water outlet Temperature
31.	XMEAS22	Separator cooling water outlet temperature

Table 2. Description of the selected data monitoring variables

The mode shift probability matrix is set as:

$A=$

0	1	0
0	0	1
0.75	0.25	0

The duration of each mode follows the Gaussian distribution $N\left(\mu_i, \sigma_i^2\right)$, where $\mu_i = [80, 60, 70]$, $\sigma_i = [10, 10, 10]$, and $D_{max} = 100$.

The training set consists of a single simulation that runs normally (healthily) for 1000 hours. The sampling time of data acquisition is 0.5 hours, which gives a set of 2000 observations. Figure 3 depicts the evolution of mode in relation to time. The evaluation is used to assess the constructed monitoring scheme and PCA model. It is used to calculate false alarms resulting from the Q and T^2 statistics. Twenty-two faults are generated by different runs and fault occurrence times; each run corresponds to one of the process faults listed in Table 3.
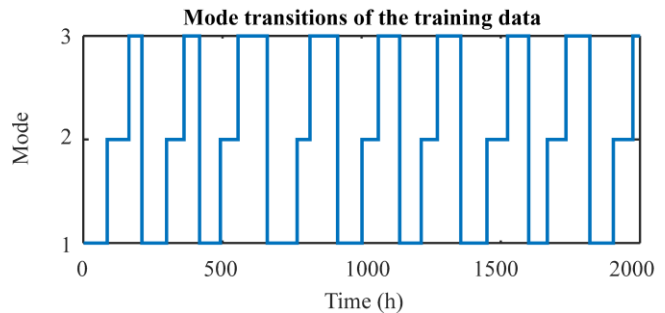
Figure 3. Mode transitions of the training data

The test set corresponds to a 300-hour operation of a healthy process. At least 600 samples exhibiting mode displacement in accordance with the probability shifting mode were observed. Figure 4 illustrates test data with fault types 9 and 20. Initially the data runs normally (solid blue line), until at a certain time a disturbance is given according to the type of fault.

Test data-9 in the figure only displays 1 sensor, in order to see the normal data process, fault data, and data taken as test data. The data starts from Mode 1, then goes to Mode 2 and Mode 3, and repeats from Mode 1. The process of generating test data follows the mode shift probability and distribution that has been defined previously. On the horizontal axis of the figure, the Mode caption indicates the Mode shift for one test data sample.

No	Description	Disturbance type	Fault begins at time
Fault-1	Feed ratio of A/C, composition constant of B (stream 4)	Step	100 h in Mode 2
Fault-2	Composition of B, ratio constant of A/C (stream 4)	Step	100 h in Mode 2
Fault-3	Feed temperature of D (stream 2)	Step	100 h in Mode 2
Fault-4	Inlet temperature of reactor cooling water	Step	100 h in Mode 2
Fault-5	Inlet temperature of condenser cooling water	Step	100 h in Mode 2
Fault-6	Header pressure loss of C—reduced availability (stream 4)	Step	100 h in Mode 2
Fault-7	Feed composite of A, B, and C on (stream 4)	Random	180 h in Mode-3
Fault-8	Feed temperature of D (stream 2)	Random	180 h in Mode-3
Fault-9	Feed temperature of C (stream 4)	Random	180 h in Mode-3
Fault-10	Inlet temperature of reactor cooling water	Random	180 h in Mode-3
Fault-11	Inlet temperature of condenser cooling water	Random	180 h in Mode-3
Fault-12	Reaction kinetics	Drift	180 h in Mode-3
Fault-13	Valve of reactor cooling water	Sticking	180 h in Mode-3
Fault-14	Valve of condenser cooling water	Sticking	250 h in Mode-1
Fault-15	(unknown); deviations of heat transfer within stripper (heat exchanger)	Random	250 h in Mode-1
Fault-16	(unknown); deviations of heat transfer within reactor	Random	250 h in Mode-1
Fault-17	(unknown); deviations of heat transfer within condenser	Random	250 h in Mode-1
Fault-18	(unknown); re-cycle valve of compressor, underflow separator (stream 10), underflow stripper (stream 11) and steam valve stripper	Sticking	250 h in Mode-1
Fault-19	(Unknown)	Random	250 h in Mode-1
Fault-20	Mode shifts from Mode-1 to Mode-3	Step	250 h in Mode-1
Fault-21	Mode shifts from Mode-1 to Mode-3	Step	50 h in Mode-1
Fault-22	Mode shifts from Mode-2 to Mode-1	Step	100 h in Mode-2

Table 3. Fault descriptions for simulations
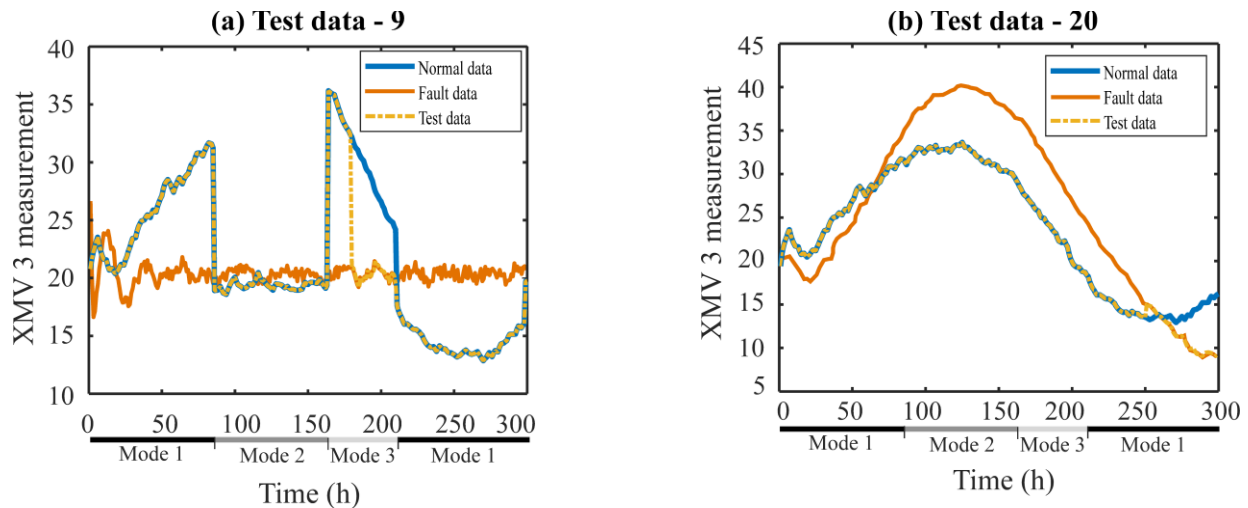
Figure 4. Transition of operating conditions of test data: (a) Fault-9 and (b) Fault-20

For example, for fault type-9, the disturbance occurs at 180 h in mode 3 (red dotted line). After mode 3 ends, the data returns to normal conditions. The test data are the orange dotted line. This test data will be used for testing. This data has 31 variables with the same fault type-9. Figure 4 (a) is an illustration of normal data, fault data and test data from

variable XMV3 for fault type 9. Fault-20 was not given any disturbance but changed from Mode-1 to Mode-3 at time 250 h (Figure 4 (b)). The system can operate in multiple modes at one time sequence. So, a change of mode at an inopportune time can lead to incorrect results. This is referred to as a system failure because the system is not working in its mode time path.

6. RESULTS AND DISCUSSION

In this section, the proposed methodology is used to address the fault detection problem of the TEP. This simulation is referred to as HSMM+PCA because the first step involves estimating the operation condition, or "State", in HSMM via Agglomerative clustering, parameter initialization, HSMM training, and decoding. The second process is PCA-based data modeling, which includes calculations of T^2, Q, T_α^2, Q_α, $T^{2,ad}$, and Q^{ad}. At the conclusion of online monitoring, four combination indices can be used to identify faults. Figure 5 shows the training data of TEP data in 1000 h time. There are several variables in the figure, namely XMV 1, XMV 2, XMV 3, XMEAS 1, and XMEAS 2. Some of these variable values are presented in the Table 4. Descriptions of the variables can be seen in Table 2.

Variable	1	2	3	…	999	1000
XMV 1	92.91	95.15	96.52	...	98.25	98.30
XMV 2	9.12	9.33	9.40	...	9.27	9.26
XMV 3	20.77	21.63	22.24	...	22.27	22.19
XMEAS 1	8.90	9.08	9.02	...	8.66	8.70
XMEAS 2	35.90	35.88	35.10	...	35.61	35.87

Table 4. Some of variables values
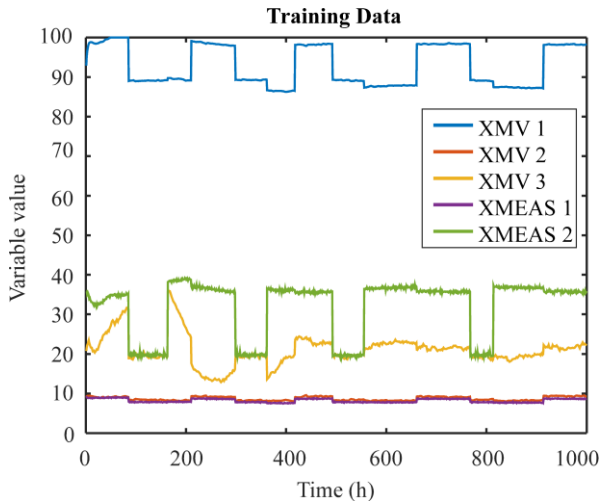
Figure 5. Training data of TEP

The results of training data (Figure 5) for 1000 hours are shown in Figure 6. The clustering result is shown in Figure 6 with a blue solid line. Using the clustering outcomes, we can

assign initial probability values to matrices B and D. The state estimation result by HSMM is depicted by the red dashed line.
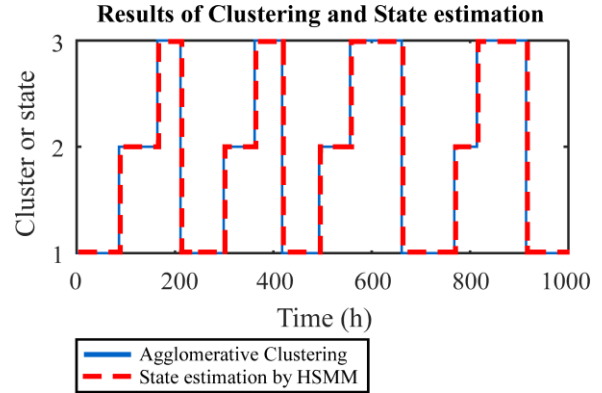
Figure 6. Clustering results using Agglomerative method and state estimation using HSMM

The calculation of Q and T^2 statistics is presented in Figure 7 (a) and 7 (a). Under normal conditions, the value of Q is below Q_α and Q^{ad}, as well as the T^2 statistic. From these values, we can get the threshold limit for normal data. In the future, we can detect abnormal conditions if the data cross this threshold. Furthermore, the test uses test data as in Table 3. Each test plan has an abnormal condition.
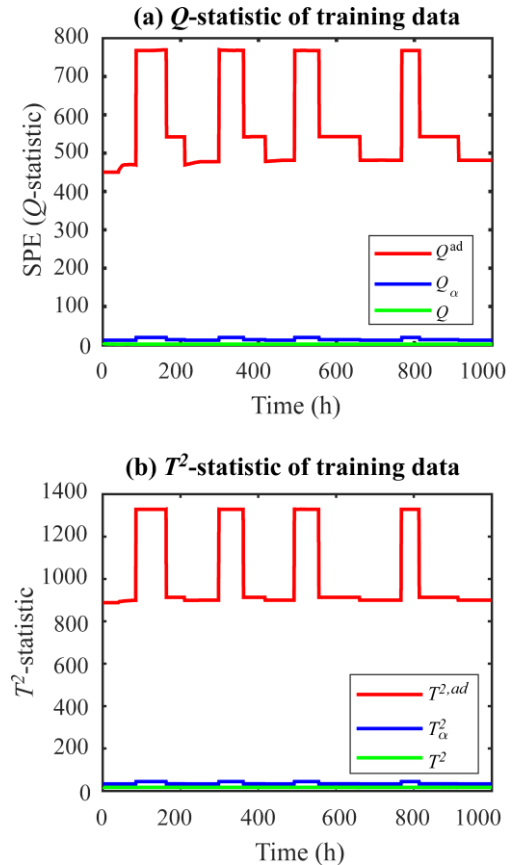
Figure 7. Plot of Q and T^2 statistic values

Figure 8 depicts the result of using HSMM to estimate the state for Fault-9 test data. For these data, HSMM estimates the state with high accuracy (94.67%).
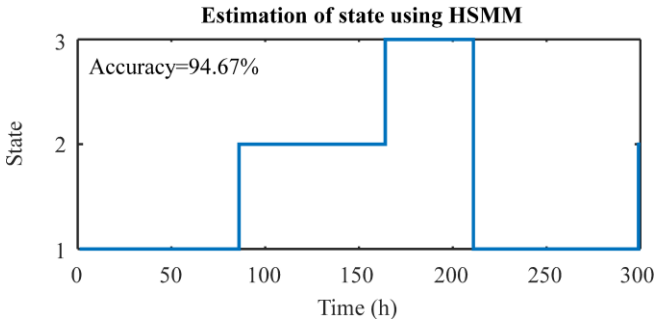
Figure 8. State estimation of test data (Fault-9) using HSMM

The TEP data test refers to the scenario described in Lou and Wang's data test scenario processes (Lou & Wang, 2017). This study introduces the HSMM-PCA method and compares it to the Mixture Bayesian PCA (MBPCA) (Ge & Song, 2010) and HMM (Wang *et al.*, 2016) methods. Consequently, it is possible to compare the simulation results with the article's findings. HSMM-PCA employs the Cumulative Index (CI), MBPCA considers T^2 and Q values, and HMM uses the Natural Logarithm of the Likelihood Probability (NLLP) index.

We detail four associations of indexes from the statistical values of T^2, Q, T^2_α, Q_α, $T^{2,ad}$, and Q^{ad}. Figure 9 and Figure 10 explains the results of detecting Fault-9 data using these methods. Figures 9 (a) to 9 (d) are the results from the article by Lou & Wang (2017), while Figures 10(a) to 10(d) are the results from this study.
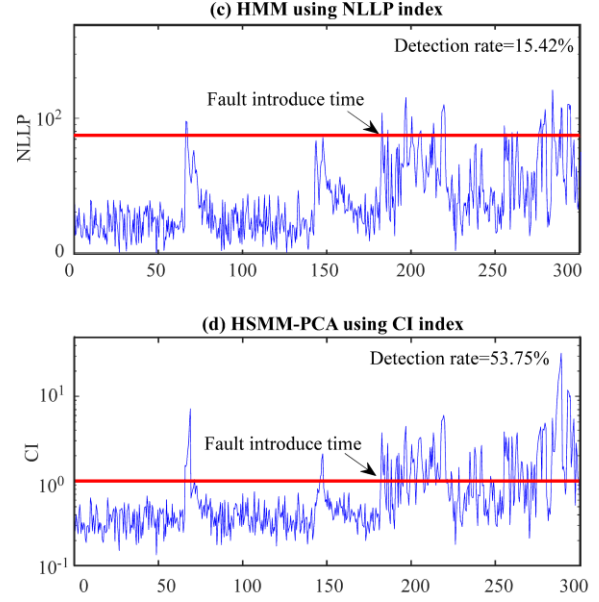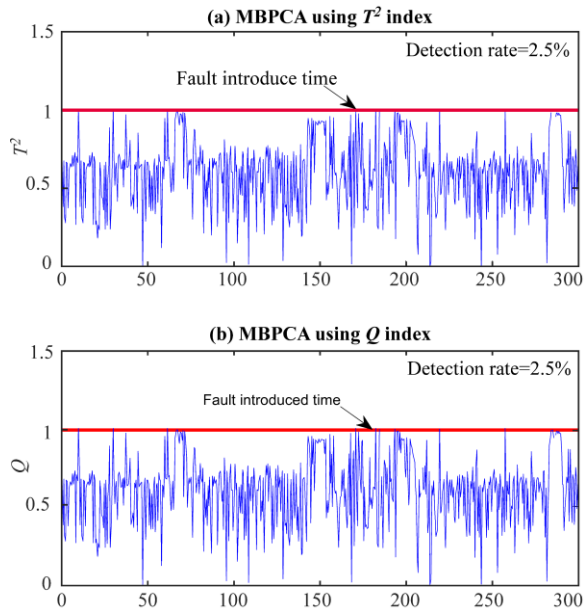
Figure 9. Fault-9 data test fault detection by Lou & Wang (2017)

False Alarm Rate (FAR) and Fault Detection Rate (FDR) are used as performance evaluation indices. FAR and FDR are detected as follows (Chen *et al.*, 2020):

$$FDR = \frac{\text{the number of faulty samples identified as fault}}{\text{the number of faulty samples}} \times 100$$

(22)

$$FAR = \frac{\text{the number of normal samples detected as faults}}{\text{the number of normal samples}} \times 100$$

(23)

The assignment of a reliable monitoring scheme is to acquire the highest FDR and lowest FAR. Faults of type 9 occurred between 180 and 210 hours. In Figure 9 (a) and 9 (b), the MBPCA method, which is based on the T^2 and Q indices, has a detection rate of 2.5% and can detect only a few faults. Fig. 9 (c) depicts the HMM method using the NLLP index, which can detect 15.42% of faults. Figure 9 (d) shows that the HSMM-PCA method employing the CI-index can detect 53.75% of faults.

10
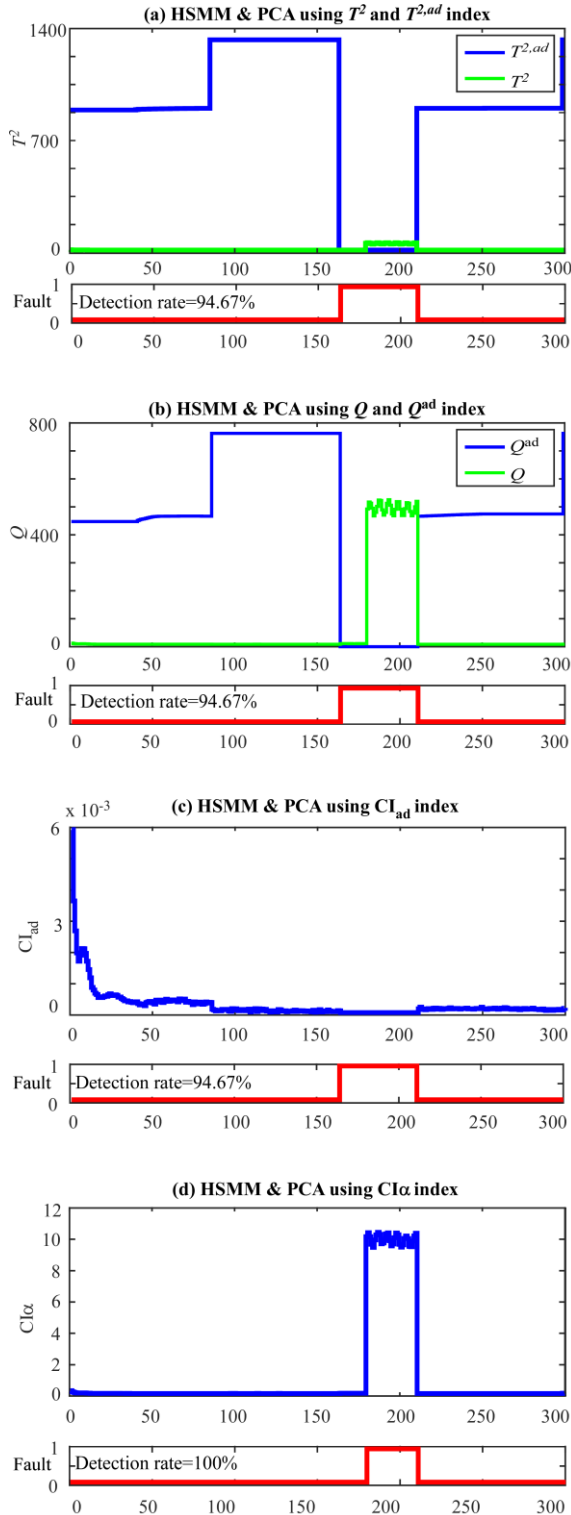
Figure 10. Fault-9 data test fault detection of this study

Our proposed method, shown in Figure 10 (a), 10 (b), and 10 (c), is effective at detecting 94.67% of faults. The adaptation factor in the monitoring performance ($T^{2,ad}$ and Q^{ad}) using the weighting factor is one ($c_q = c_t = 1$) and window length is 40

($w_q = w_t = 40$). These values were obtained from several experiments that gave the best detection rate results. In particular, the CI_α index can detect complete failure (Figure 10 (d)). The *threshold* used for indexing using CI_α is 0.2 which is obtained from experimental results. This is a weakness in this research. Because some of the values above are determined from trial results until finding the highest FDR results. We have not been able to formulate a methodology for determining it automatically.

Figures 11 (a) to 11 (d) are the results from the article by Lou & Wang (2017), while Figures 12 (a) to 12 (d) are the results from this study for fault type 20.
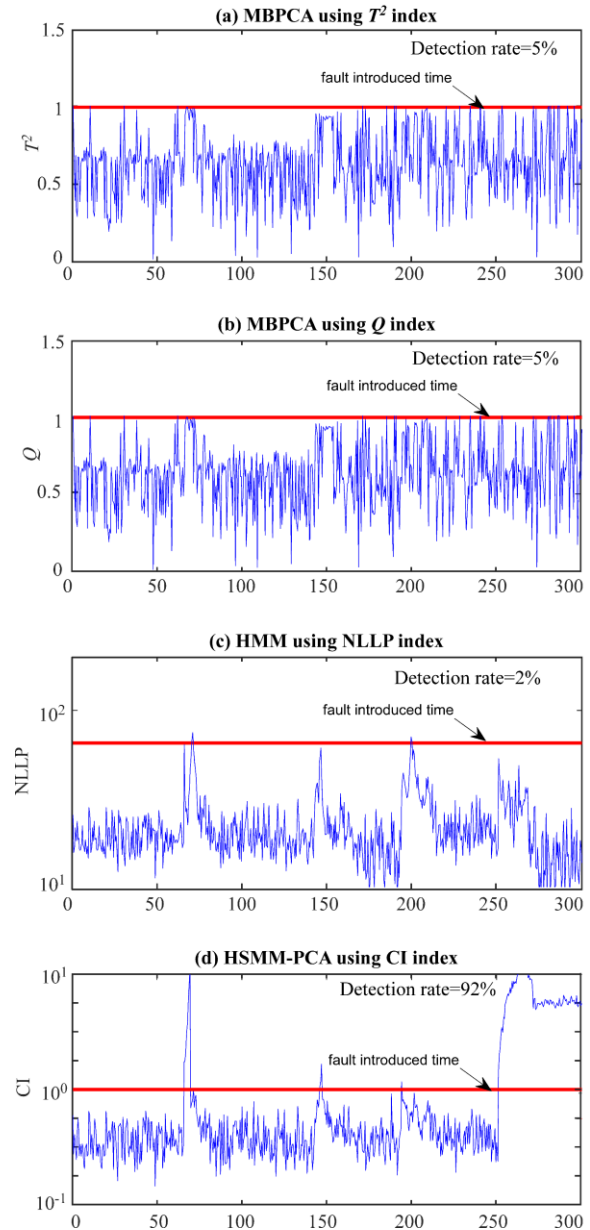
Figure 11. Fault-20 data test fault detection (Lou & Wang, 2017)

11
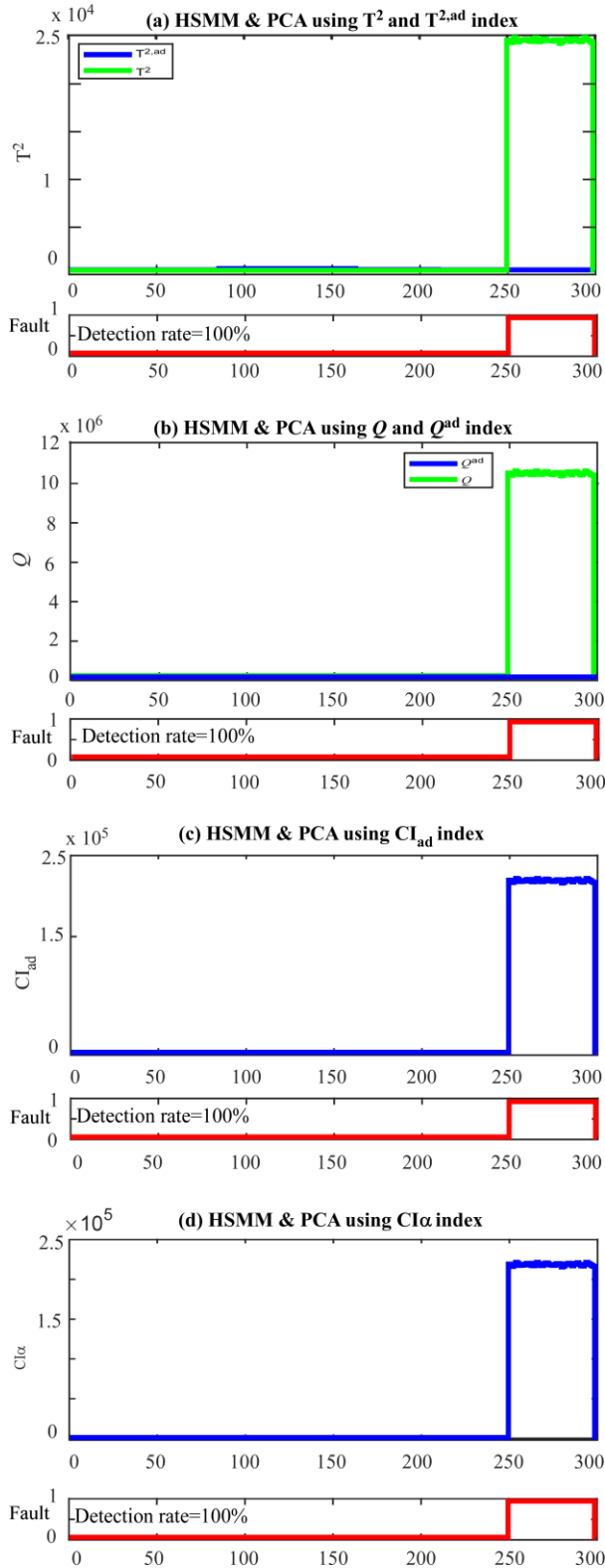
Figure 12. Fault-20 data test fault detection of this study

In fault type 20, faults occurred between 250 h and 300 h. Figure 11 (c) depicts the HMM method using the NLLP index, which can detect 2% of faults. The MBPCA method,

which is based on the T^2 and Q indexes, has a detection rate of 5%, as shown in Figure 11 (a) and 11 (b). Figure 11 (d) shows that the HSMM-PCA method using the CI-index can detect 92% of faults. Our proposed method, HSMM+PCA using four index types shown in Figure 12 (a) until 12 (d), is 100% successful in detecting faults.

The detection rates of the four methods are listed in Table 4. The results of this method are compared with previous results using the HMM, MBPCA, and HSMM-PCA methods from Lou and Wang (2017). The MBPCA method using the T^2 index yielded the lowest FDR of 8.42%, while the Q index contributed an average value of 25.58%. The HMM method had a mean detection rate of 45.51 percent. The HSMM-PCA method increased the mean FDR to 67.45%. Our proposed method, HSMM+PCA, has an average FDR of 93.85%, 98.27%, 98.30%, and 100% for the four index types. The CI_α index is 100% effective at detecting errors. The average false alarm rate for all defects is shown in Table 4.

In the last part of Table 5, note * sourced from (Lou & Wang, 2017). Some faults are almost completely undetected, and only few faults are 100% detected. It is due to the lack of success in HMM and HSMM decoding causing errors during monitoring, and the inability of the index to assist in the discovery of error thresholds. Therefore, we proposed HSMM method, more efficient in decode, combined fixed and adaptive thresholds of PCA statistics for monitoring. In our research, it successfully detected many faults with 100% rate. If we compared our work with to the paper (Lou & Wang, 2017), there are 3 differences with this contribution. First for HSMM formula, authors proposed his own formula to get the value of the observation's probability distribution (parameter B, see formula 7, (Lou & Wang, 2017). In our study, we used clustering (Agglomerative) to get the initial B.

Then, we used Forward-Backward HSMM for multiple observations by adding the calculation of the probability function of the observation sequence (see algorithm: FB HSMM). The HSMM decoding results obtained are therefore different. In Lou (2017), we noted many problems in HSMM decoding results due to the observation probability value (B matrix). Second for the online monitoring stage, authors used the affiliation probability value (γ) in the calculation of T^2 and SPE (see formula 19 in (Lou & Wang, 2017)). In fact, due to the previous decoding error of HSMM, this value can affect the assessment of statistical data. Of course, the monitoring results will be less precise. Finally, authors only used a cumulative index that combined 2 statistical values. Whereas we used multiple monitoring indices to provided better detection rate results.

Test data	HMM*	MBPCA*		HSMM-PCA*	HSMM+PCA			
	NLLP	Q	T^2	CI	T^2 and $T^{2,ad}$	Q and Q^{ad}	CI_{ad}	CI_α
Fault-1	100.00	99.50	2.00	100.00	100.00	100.00	100.00	100
Fault-2	97.25	65.75	20.25	98.50	100.00	100.00	100.00	100
Fault-3	0.75	1.50	2.00	3.50	100.00	100.00	100.00	100
Fault-4	76.25	1.50	2.25	99.75	100.00	100.00	100.00	100
Fault-5	1.50	1.50	3.00	3.75	100.00	100.00	100.00	100
Fault-6	100.00	95.75	3.00	100.00	100.00	100.00	100.00	100
Fault-7	96.25	59.80	15.00	98.33	94.67	94.67	94.67	100
Fault-8	2.92	2.50	3.33	4.58	94.67	94.67	94.67	100
Fault-9	15.42	2.50	2.50	53.75	94.67	94.67	94.67	100
Fault-10	80.83	3.75	2.08	97.50	94.67	94.67	94.67	100
Fault-11	2.50	2.50	2.50	12.08	94.67	94.67	94.67	100
Fault-12	96.25	91.25	72.80	97.92	94.67	94.67	94.67	100
Fault-13	78.33	2.50	2.08	95.42	94.67	94.67	94.67	100
Fault-14	1.00	6.00	2.00	9.00	83.67	100.00	100.00	100
Fault-15	1.00	6.00	2.00	9.00	83.67	100.00	100.00	100
Fault-16	71.00	9.00	3.00	89.00	83.67	100.00	100.00	100
Fault-17	57.00	10.00	6.00	77.00	83.67	100.00	100.00	100
Fault-18	17.00	6.00	1.00	83.00	83.67	100.00	100.00	100
Fault-19	97.00	70.00	29.00	97.00	83.67	100.00	100.00	100
Fault-20	2.00	5.00	5.00	92.00	100.00	100.00	100.00	100
Fault-21	1.00	12.60	2.28	62.80	100.00	99.33	100.00	100
Fault-22	6.00	7.75	2.25	100.00	100.00	100.00	100.00	100
Mean FDR	45.51	25.58	8.42	67.45	93.85	98.27	98.30	100
Mean FAR	0.03	0 .05	2.00	0.07	1.80	1.92	1.80	0

Note: * Sourced from (Lou & Wang, 2017)

Table 5. Detection rates (%) of simulations in TEP

7. CONCLUSION

In this study, HSMM and PCA were combined to monitor an industrial process that uses multiple operational settings. The HSMM method successfully identified the mode of a system with a multi-mode process. Agglomerative clustering is efficient for dividing data and supports HSMM learning for the initial setting of HSMM parameters. The PCA model performs data monitoring for each mode. HSMM+PCA uses mode shift probability and duration for mode identification and online monitoring. This makes it possible to find mode issues that confound earlier multimode techniques. The use of combination indexes of T^2, Q, T_α^2, Q_α, T_{ad}^2, and Q_{ad} can enhance the fault detection rate. The combination indexes named CI_{ad} and CI_α successfully detected faults. This is verified in the revised Tennessee Eastman process. The test result for the TEP indicates that HSMM+PCA is excellent and robust. The mean fault detection ratio is 100%. It is proven that this method can improve failure detection. Many parameters need to be set, namely the initialization of HSMM parameters. These are obtained automatically by the clustering method. While the adaptive parameters in the monitoring process (weighting factor and window length), and the threshold value in the fault detection process are still supervised. These values are based on trial results until finding the highest FDR. This is a limitation of the proposed method.

REFERENCES

Alkaya, A., & Eker, I. (2011). Variance sensitive adaptive threshold-based PCA method for fault detection with experimental application. *ISA Trans*, *50*(2), 287-302. https://doi.org/10.1016/j.isatra.2010.12.004

Atamuradov, V., Medjaher, K., Dersin, P., Lamoureux, B., & Zerhouni, N. (2017). Prognostics and health management for maintenance practitioners-Review, implementation and tools evaluation. *International Journal of Prognostics and Health Management*, *8*(3), 1-31.

Bakdi, A., & Kouadri, A. (2018). An improved plant-wide fault detection scheme based on PCA and adaptive threshold for reliable process monitoring: Application on the new revised model of Tennessee Eastman process. *Journal of Chemometrics*, *32*(5), e2978. https://doi.org/10.1002/cem.2978

Bathelt, A., Ricker, N. L., & Jelali, M. (2015). Revision of the Tennessee Eastman process model. *IFAC-PapersOnLine*, *48*(8), 309-314.

Chen, Z., Liu, C., Ding, S. X., Peng, T., Yang, C., Gui, W., & Shardt, Y. A. (2020). A just-in-time-learning-aided canonical correlation analysis method for multimode process monitoring and fault detection. *IEEE Transactions on Industrial Electronics*, *68*(6), 5259-5270.

Downs, J. J., & Vogel, E. F. (1993). A plant-wide industrial process control problem. *Computers & chemical engineering*, *17*(3), 245-255.

Galagedarage Don, M., & Khan, F. (2019). Process fault prognosis using hidden Markov model–bayesian networks hybrid model. *Industrial & Engineering Chemistry Research*, *58*(27), 12041-12053.

Ge, Z., & Song, Z. (2010). Mixture Bayesian regularization method of PPCA for multimode process monitoring. *AIChE journal*, *56*(11), 2838-2849.

Jiang, Q., Yan, X., & Huang, B. (2019). Review and perspectives of data-driven distributed monitoring for industrial plant-wide processes. *Industrial & Engineering Chemistry Research*, *58*(29), 12899-12912.

Jolliffe, I. T., & Cadima, J. (2016). Principal component analysis: a review and recent developments. *Philosophical Transactions of the Royal Society A: Mathematical, Physical and Engineering Sciences*, *374*(2065), 20150202. https://doi.org/10.1098/rsta.2015.0202

Kong, X., & Ge, Z. (2021). Deep learning of latent variable models for industrial process monitoring. *IEEE Transactions on Industrial Informatics*, *18*(10), 6778-6788.

Kulkarni, A., Jayaraman, V. K., & Kulkarni, B. D. (2005). Knowledge incorporated support vector machines to detect faults in Tennessee Eastman Process.

Computers & chemical engineering, *29*(10), 2128-2133.

Liu, T., & Zhu, K. (2020). A switching hidden semi-Markov model for degradation process and its application to time-varying tool wear monitoring. *IEEE Transactions on Industrial Informatics*, *17*(4), 2621-2631.

Lou, Z., & Wang, Y. (2017). Multimode continuous processes monitoring based on hidden semi-Markov model and principal component analysis. *Industrial & Engineering Chemistry Research*, *56*(46), 13800-13811.

Md Nor, N., Che Hassan, C. R., & Hussain, M. A. (2020). A review of data-driven fault detection and diagnosis methods: Applications in chemical process systems. *Reviews in Chemical Engineering*, *36*(4), 513-553.

Nawaz, M., Maulud, A. S., Zabiri, H., Taqvi, S. A. A., & Idris, A. (2021). Improved process monitoring using the CUSUM and EWMA-based multiscale PCA fault detection framework. *Chinese Journal of Chemical Engineering*, *29*, 253-265.

Nielsen, F. (2016). Hierarchical clustering. In *Introduction to HPC with MPI for Data Science* (pp. 195-211). Springer.

Odiowei, P.-E. P., & Cao, Y. (2009). Nonlinear dynamic process monitoring using canonical variate analysis and kernel density estimations. *IEEE Transactions on Industrial Informatics*, *6*(1), 36-45.

Peng, X., Tang, Y., Du, W., & Qian, F. (2017). Multimode process monitoring and fault detection: A sparse modeling and dictionary learning method. *IEEE Transactions on Industrial Electronics*, *64*(6), 4866-4875.

Pratley, A., van Voorthuysen, E., & Chan, R. (2015). A step-by-step approach for modelling complex systems with Partial Least Squares. *Proceedings of the Institution of Mechanical Engineers, Part B: Journal of Engineering Manufacture*, *229*(5), 847-859.

Quatrini, E., Costantino, F., Di Gravio, G., & Patriarca, R. (2020). Condition-based maintenance—an extensive literature review. *Machines*, *8*(2), 31. https://doi.org/10.3390/machines8020031

Reinartz, C., Kulahci, M., & Ravn, O. (2021). An extended Tennessee Eastman simulation dataset for fault-detection and decision support systems. *Computers & chemical engineering*, *149*, 107281.

Tamssaouet, F., Nguyen, T. K., Medjaher, K., & Orchard, M. E. (2019). Uncertainty quantification in system-level prognostics: application to Tennessee Eastman process. 2019 6th International Conference on Control, Decision and Information Technologies (CoDIT),

Vrignat, P., Kratz, F., & Avila, M. (2022). Sustainable manufacturing, maintenance policies, prognostics and health management: A literature review.

Reliability Engineering & System Safety, *218*, 108140. https://doi.org/10.1016/j.ress.2021.108140

Wang, F., Tan, S., Yang, Y., & Shi, H. (2016). Hidden Markov model-based fault detection approach for a multimode process. *Industrial & Engineering Chemistry Research*, *55*(16), 4613-4621.

Wu, P., Lou, S., Zhang, X., He, J., & Gao, J. (2020). Novel quality-relevant process monitoring based on dynamic locally linear embedding concurrent canonical correlation analysis. *Industrial & Engineering Chemistry Research*, *59*(49), 21439-21457.

Xia, Y., Wang, W., Song, Z., Xie, Z., Chen, X., & Li, H. (2021). Fault diagnosis of flexible production line machining center based on PCA and ABC-LVQ. *Proceedings of the Institution of Mechanical Engineers, Part B: Journal of Engineering Manufacture*, *235*(4), 594-604.

Yu, S.-Z., & Kobayashi, H. (2003). An efficient forward-backward algorithm for an explicit-duration hidden Markov model. *IEEE signal processing letters*, *10*(1), 11-14. https://doi.org/10.1109/LSP.2002.806705

Zhang, H., Chen, H., Guo, Y., Wang, J., Li, G., & Shen, L. (2019). Sensor fault detection and diagnosis for a water source heat pump air-conditioning system based on PCA and preprocessed by combined clustering. *Applied Thermal Engineering*, *160*, 114098.

BIOGRAPHIES

Lestari Handayani received the Ph.D. degree from INSA Centre Val de Loire, France, since 2022. She is currently an Assistant Professor at the Department of Informatics Engineering, Universitas Islam Negeri Sultan Syarif Kasim Riau, Indonesia. She is also the head of the Artificial Intelligent of Things (AIoT) research team. Her research areas include the study of Prognostics and Health Management, pattern recognition, signal processing techniques, image processing, data mining, and Artificial Intelligent.

Pascal Vrignat received his Ph.D. degree in automatics from the doctoral school of science and technology, Orleans University, France, in 2010. His research focuses on dependability, diagnosis, prognosis and maintenance strategies for systems (Markovian and stochastic processes). His main work in teaching for the industry of the future concerns: the development of applications in industrial data processing for industrial processes, the control-command of the processes (local or remote) associating applications of Human-Machine interfaces, and supervisors (Supervisory Control and Data Acquisition & Industry 4.0 applications). He was awarded the SAGE Best Paper Prize in 2012 by the editorial board of the Journal of Risk and Reliability.

Frédéric Kratz received his Ph. D degree in control engineering from the University Henri Poincaré of Nancy, France, in 1991. He received the French Habilitation degree from the Institut National Polytechnique de Lorraine (INPL), France, in 1998. He is currently a Professor with the Department of Industrial Risk Control, INSA Centre Val de Loire, Bourges, France. He is also a Research Director at PRISME Laboratory. His current research interests concern diagnosis, estimation, prognosis and reliability engineering of automatic control systems.